NACA RM L56A17

NACA

RESEARCH MEMORANDUM

LATERAL STABILITY CHARACTERISTICS BETWEEN MACH NUMBERS OF 0.80 AND 1.57 AND SIMULATION OF COUPLED MOTION AT MACH NUMBER 1.30 OF A ROCKET-PROPELLED MODEL OF AN AIRPLANE CONFIGURATION HAVING THIN HIGHLY TAPERED 45° SWEPTBACK SURFACES

By Charles T. D'Aiutolo and Allen B. Henning

Langley Aeronautical Laboratory
Langley Field, Va.

NATIONAL ADVISORY COMMITTEE FOR AERONAUTICS

WASHINGTON

April 10, 1956
Declassified January 20, 1958

NATIONAL ADVISORY COMMITTEE FOR AERONAUTICS

RESEARCH MEMORANDUM

LATERAL STABILITY CHARACTERISTICS BETWEEN MACH NUMBERS OF 0.80 AND 1.57 AND SIMULATION OF COUPLED MOTION AT MACH NUMBER 1.30 OF A ROCKET-PROPELLED MODEL OF AN AIRPLANE CONFIGURATION HAVING THIN HIGHLY TAPERED 45° SWEPTBACK SURFACES

By Charles T. D'Aiutolo and Allen B. Henning

SUMMARY

A rocket-propelled model of an airplane configuration having thin, highly tapered, 45° sweptback surfaces was tested in the Mach number range of 0.80 to 1.57 to obtain the lateral stability characteristics of the configuration.

The results of the analysis of the Dutch roll oscillations indicated that from Mach number 1.3 to 1.57, the lateral-force derivative decreased and the directional stability was relatively constant. At a Mach number of 1.50, the value of the directional-stability derivative as obtained from the application of the time-vector method agreed with the value as obtained from the single-degree-of-freedom method.

At a Mach number of 1.3 (a dynamic pressure of 2,060 pounds per square foot), the model experienced a violent combined lateral-longitudinal motion, and large angles of attack and sideslip together with large rolling velocities were recorded. Approximate simulation of this combined motion on an analog computer using nonlinear equations of motion with five degrees of freedom was made and indicated possible values of the stability derivatives of the model while performing the roll-induced excursions in angle of attack and angle of sideslip.

INTRODUCTION

A systematic investigation of the dynamic lateral stability characteristics of airplane configurations at high subsonic, transonic, and

supersonic speeds is being conducted by the Langley Pilotless Aircraft Research Division by means of rocket-propelled models. Initial results of this investigation have been published in references 1 and 2 where the dynamic lateral stability characteristics of a swept-wing configuration (ref. 1) and a straight-wing configuration (ref. 2) are presented.

This report contains the results of a flight test to determine the dynamic lateral stability characteristics of a rocket-propelled model of an airplane configuration having thin, highly tapered, 45° sweptback surfaces. The Mach number range covered in this test was from 0.80 to 1.57 and corresponds to a Reynolds number range (based on wing mean aerodynamic chord) of 6.7×10^6 to 13.3×10^6, respectively. The model was flown at the Langley Pilotless Aircraft Research Station at Wallops Island, Va.

Stability derivatives were determined by analyzing the oscillations in yaw by means of the time-vector method as applied to rocket-propelled models. (See refs. 1 and 2). These oscillations were produced by the firing of pulse rocket motors.

During the test, the model experienced a violent lateral-longitudinal coupled motion and large angles of attack and sideslip were recorded at high roll rates. A simulation study of this coupled motion was performed on an analog computer to determine the stability derivatives of the model during this maneuver.

SYMBOLS AND COEFFICIENTS

In this paper the forces and moments acting on the model are referred to the body system of axes shown in figure 1 and may be transposed to the stability system of axes by use of the expressions derived in reference 3. The origin of the axes system was at the center of gravity of the model which was coincident with the 0.193 mean aerodynamic chord of the wing. The symbols and coefficients are defined as follows:

a	total damping factor (logarithmic decrement of Dutch roll oscillation defined as being a positive number for a damped oscillation)
A_{T}/g	acceleration along Y-reference axis as obtained from accelerometer, positive to the right.
b	wing span, ft
b_t	horizontal-tail span, ft

$\bar{c}$	mean aerodynamic chord, ft
I_X	moment of inertia about body X-axis, slug-ft^2
I_Y	moment of inertia about body Y-axis, slug-ft^2
I_Z	moment of inertia about body Z-axis, slug-ft^2
I_{XZ}	product of inertia in XZ-plane referred to body axes system (positive when the positive direction of the X-principal axis is inclined below the reference axis.)
L	rolling moment, ft-lb
M'	pitching moment, ft-lb
N	yawing moment, ft-lb
M	Mach number
m	mass of model, slugs
P	period of the Dutch roll oscillation, sec
p,q,r	angular velocities about X, Y, and Z body axes, radians/sec
q_o	dynamic pressure, $\frac{1}{2}\rho V^2$, lb/sq ft
R	Reynolds number
S	total wing, area, sq ft
V	velocity, ft/sec
W	model weight, lb
$\frac{y}{b_{t/2}}$	nondimensional lateral coordinate with respect to the tail span
$\frac{z}{b/2}$	nondimensional vertical coordinate with respect to the wing span
ρ	air density, slugs/cu ft
μ	relative density factor, $\frac{m}{\rho S b}$

ω natural circular frequency of the Dutch roll oscillation, radians/sec

α angle of attack, deg or radians

β angle of sideslip, deg or radians

ϵ downwash angle, deg

θ angle of pitch, deg

ϕ angle of roll, radians

ψ angle of yaw, radians

σ angle of sidewash, deg

Φ phase angle, deg

Λ sweep angle of quarter-chord line, deg

Δ incremental change in quantity

ω_ψ^2 square of the nondimensional undamped natural frequency in yaw, $\frac{C_{n_\beta} qSb}{I_Z p^2}$

ω_θ^2 square of the nondimensional undamped natural frequency in pitch, $\frac{C_{m_\alpha} qS\bar{c}}{I_Y p^2}$

ζ_ψ fraction of critical damping ratio in yaw

ζ_θ fraction of critical damping ratio in pitch

C_L lift coefficient, Lift/$q_o S$

C_Y lateral-force coefficient, Lateral force/$q_o S$

C_m pitching-moment coefficient, Pitching moment/$q_o S\bar{c}_w$

C_n yawing-moment coefficient, Yawing moment/$q_o Sb$

C_l rolling-moment coefficient, Rolling moment/q_oSb

C_{n_β} directional-stability derivative, $\partial C_n/\partial\beta$, per radian

C_{Y_β} lateral-force derivative, $\partial C_Y/\partial\beta$, per radian

C_{l_β} effective dihedral derivative, $\partial C_l/\partial\beta$, per radian

C_{n_p} rate of change of yawing-moment coefficient with rolling-angular-velocity factor, $\frac{\partial C_n}{\partial\left(\frac{pb}{2V}\right)}$, per radian

C_{Y_p} rate of change of lateral-force coefficient with rolling-angular-velocity factor, $\frac{\partial C_Y}{\partial\left(\frac{pb}{2V}\right)}$, per radian

C_{l_p} damping-in-roll derivative, $\frac{\partial C_l}{\partial\left(\frac{pb}{2V}\right)}$, per radian

C_{n_r} rate of change of yawing-moment coefficient with yawing-angular-velocity factor, $\frac{\partial C_n}{\partial\left(\frac{rb}{2V}\right)}$, per radian

C_{Y_r} rate of change of lateral-force coefficient with yawing-angular-velocity factor, $\frac{\partial C_Y}{\partial\left(\frac{rb}{2V}\right)}$, per radian

C_{l_r} rate of change of rolling-moment coefficient with yawing-angular-velocity factor, $\frac{\partial C_l}{\partial\left(\frac{rb}{2V}\right)}$, per radian

$C_{n_{\dot\beta}}$ rate of change of yawing-moment coefficient with rate of change of angle-of-sideslip factor, $\frac{\partial C_n}{\partial\left(\frac{\dot\beta b}{2V}\right)}$, per radian

$C_{Y_{\dot{\beta}}}$ rate of change of lateral-force coefficient with rate of change of angle-of-sideslip factor, $\frac{\partial C_Y}{\partial\left(\frac{\dot{\beta}b}{2V}\right)}$, per radian

$C_{l_{\dot{\beta}}}$ rate of change of rolling-moment coefficient with rate of change of angle-of-sideslip factor, $\frac{\partial C_l}{\partial\left(\frac{\dot{\beta}b}{2V}\right)}$, per radian

C_{m_β} rate of change of pitching-moment coefficient with angle of sideslip, $\partial C_m/\partial\beta$, per radian

C_{L_α} lift-curve slope, $\partial C_L/\partial\alpha$, per radian

C_{m_q} rate of change of pitching-moment coefficient with pitching-angular-velocity factor, $\frac{\partial C_m}{\partial\left(\frac{q\bar{c}}{2V}\right)}$, per radian

C_{m_α} slope of pitching-moment curve, $\partial C_m/\partial\alpha$, per radian

$C_{m_{\dot{\alpha}}}$ rate of change of pitching-moment coefficient with rate of change of angle-of-attack factor $\frac{\partial C_m}{\partial\left(\frac{\dot{\alpha}\bar{c}}{2V}\right)}$, per radian

C_D drag coefficient, Drag/q_oS

Subscripts:

W wing

VT vertical tail

PR pulse rocket

The symbol $|\ |$ represents the absolute magnitude of the quantity and is always taken to be positive. A dot over a variable indicates the first derivative of the variable with respect to time. Two dots indicate the second derivative with respect to time. The second subscript symbol

of the phase angles is used as a reference. A positive sign associated with the phase angle indicates that the first subscript symbol leads the reference, whereas a negative sign indicates that the first subscript symbol lags the reference.

MODEL, INSTRUMENTATION, AND TEST DESCRIPTION

Model Description

The general arrangement of the model is shown in figure 2, and the geometric and mass characteristics of the model are given in table I. Photographs of the model and the model-booster combination are shown in figure 3.

The fuselage was essentially a body of revolution and consisted of an ogival nose section, a cylindrical body section with rather large wing-root fairings for structural purposes, and a straight tapered afterbody section. The nose section contained the telemeter; the center section contained the wing and necessary wing-root fairings; the afterbody section contained the horizontal and vertical tail surfaces. The fuselage was constructed of aluminum alloy with magnesium skin.

The wing of the model was mounted along the fuselage reference line. It was made of aluminum and had NACA 65A004 airfoil sections parallel to the free stream. It incorporated 45° of sweepback along the quarter-chord line, and had an aspect ratio of 4 and a taper ratio of 0.2. The geometry of the horizontal tail was identical to the wing and it was mounted in the wing-chord plane extended.

The vertical tail had an aspect ratio of 1.59 (based on the area to the fuselage center line), and contained NACA 65A004 airfoil sections parallel to free stream. It incorporated 45° of sweepback along the quarter-chord line, and had a taper ratio of 0.17.

Instrumentation

The model contained a standard NACA ten-channel telemeter. Measurements were made of the normal, longitudinal, and transverse accelerations near the center of gravity of the model. Rolling velocity was measured by means of a gyro-type instrument alined so that it was sensitive to velocities about the X-reference axis. The angle of attack and angle of sideslip were measured by an air-flow direction indicator located on a sting forward of the nose of the model. An air-flow direction indicator was also located in the plane of symmetry, above and ahead of the

horizontal tail and slightly forward of the vertical tail so that the flow angularities at a point near the vertical tail could be measured. (See figs. 2 and 3.) Total pressure was measured by a tube located on a strut mounted on the underside of the cylindrical section of the fuselage and by a tube located at a point above and to one side of the tapered afterbody section of the fuselage between the horizontal and vertical tails (see figs. 2 and 3).

In addition to measurements by the telemeter system, additional ground instrumentation was used. A rollsonde was used to measure the rate of roll of the model by means of polarized radio waves and the position of the model in space was determined by use of an NACA modified SCR 584 tracking radar set and the velocity of the model was obtained by use of the CW Doppler velocimeter radar set. Atmospheric data were obtained from a radiosonde released immediately before the model flight. Fixed and tracking motion-picture cameras were used to observe the condition of the model during most of the flight.

Preflight Tests

Prior to flight testing the mass and inertia characteristics of the model were determined (see table I). The model was also suspended by shock chords and shaken by means of an electromagnetic shaker. This preflight test was performed to determine the structural natural frequencies of the model and these characteristics are also shown in table I.

Flight Test

The model was boosted to a Mach number of 1.62 and upon burnout of the booster rocket motor the model separated from the booster. After complete separation at a Mach number of 1.57 the model was disturbed in yaw by a series of four pulse-rocket motors. These rocket motors were located in the tapered afterbody section of the model (see fig. 2) and provided thrust normal to the XZ-plane. The pulse rocket motors which had about 20 lb-sec impulse with a normal burning time of 0.06 second were timed to fire in sequence during the decelerating portion of the flight. The time histories of the resulting model motions were obtained by means of the NACA telemeter and instrument system.

The flight conditions of the model are presented in figure 4 where the variation of air density, velocity, dynamic pressure, and relative density factor with Mach number are shown. These quantities are presented so that a possible correlation of the data obtained from this test with data obtained from other tests may be made. The range of the Reynolds numbers of the present test is shown in figure 5.

ACCURACY AND CORRECTIONS

Accuracy

The estimated probable errors in the measured quantities are shown in table II. Some or all of these measured quantities are reflected directly into the lateral stability derivatives C_{Y_β}, C_{n_β}, C_{l_β}, C_{l_p}, and $C_{n_r} - C_{n_{\dot{\beta}}}$. The probable error in any one of the above derivatives due to all of the probable errors in table II was determined by the method shown in reference 2, and at a Mach number of 1.50 the accuracies of the derivatives are: 3 percent for C_{Y_β}, 7 percent for C_{n_β} and C_{l_β}, 13 percent for C_{l_p}, and 25 percent for $C_{n_r} - C_{n_{\dot{\beta}}}$. The absolute values of these derivatives are as good as or better than the values indicated above.

Corrections

The readings of the air-flow direction indicator mounted in front of the model were corrected to the model center of gravity in order to determine the angles of attack and sideslip. Also the readings of the air-flow direction indicator mounted slightly forward of the vertical tail were corrected for model rotations so that when these readings were compared with the readings of the air-flow direction indicator mounted in front of the model (corrected to the center of gravity), the flow angularity at a point near the vertical tail could be determined. These corrections were made by considering flight-path curvature effects as shown in reference 4.

The accelerometers were mounted as close as possible to the center of gravity of the model and values obtained from these instruments were corrected for the model motions in order to determine the accelerations of the center of gravity of the model.

Frequency-response corrections to all instruments were not necessary and the model natural frequency was less than 4 percent of any instrument natural frequency.

RESULTS AND DISCUSSION

Time History

The time history of the lateral motions experienced by the model due to the yaw disturbances produced by the firing of the pulse rocket motors is shown in figure 6 where the variation with time of the Mach number, rolling velocity, lateral force, angle of sideslip, and the angle of attack are presented.

The model separated from the booster at 3.45 seconds corresponding to a Mach number of about 1.57, which resulted in an angle of attack as well as a yaw and a roll disturbance to the model. (See fig. 6.) It is believed that this angle-of-attack change was small enough to have a negligible effect on the lateral motions. At $t = 4.14$ seconds ($M = 1.44$) the first pulse rocket fired and an induced angle-of-attack oscillation was recorded. This angle-of-attack oscillation quickly subsided and the model oscillated essentially in yaw. The gyro-type instrument used to measure rolling velocity became inoperative immediately upon the firing of the first pulse rocket and accurate values of the rolling velocity could not be determined after this time. The second pulse rocket motor fired at $t = 5.12$ seconds ($M = 1.30$) and a violent combined lateral-longitudinal motion occurred in which an angle of sideslip of about 8° was recorded and an angle of attack greater than the 7° instrument range was attained. In order to determine the rate of roll during this coupled motion, the readings of the rollsonde were used. (See ref. 5.) At best, the rollsonde can determine the magnitude of the roll rate, but does not accurately determine the phase between the roll rate and the angle of sideslip. A comparison was made of the roll rate as measured by the gyro-type instrument before it failed and the rollsonde to determine the accuracy of the magnitude of the roll rate as determined by the rollsonde. This comparison is shown in figure 6 (note that the gyro rolling-velocity scale is magnified). Reference 5 indicates that the rate of roll as determined from a rollsonde is least accurate when the rate of roll is changing rapidly. On this basis then, the rate of roll data shown in figure 6 when the rate of roll is changing rapidly is subject to considerable error and should be interpreted as showing only a trend. Therefore, during the combined lateral-longitudinal motion the roll rate built up rapidly and a value of about -45 radians/second was attained.

At $t = 5.40$ seconds ($M = 1.24$) the third pulse rocket fired and the angle of sideslip decreased rapidly and oscillated at relatively low amplitude. The rate of roll increased somewhat and then decreased considerably, but the angle of attack remained above the limit of the instrument range (7°). (See fig. 6.) The model was still experiencing

a combined lateral-longitudinal motion as shown by the frequency of the lateral oscillations and the magnitudes of the angle of attack and rolling velocity.

The fourth pulse rocket fired at $t = 6.67$ seconds ($M = 0.88$) and the rate of roll decreased rapidly. Also the angle of attack decreased rapidly and tended to subside. At this time the model experienced a lateral disturbance with very little pitch coupling.

From the time history of the lateral motions without pitch coupling present, the periods of the Dutch roll oscillation were determined and are shown in figure 7. These periods were determined from the oscillations in angle of sideslip, lateral force coefficient, and roll velocity. In the Mach number range where pitch coupling was present, the periods were calculated by two methods. The first method considered only the basic frequency, whereas the second method considered the rolling frequency as well as the basic frequency. (See ref. 6.) These data are also shown in figure 7 for Mach numbers at which the roll frequency could be accurately determined. The trend of the data indicates that the period decreases with increasing Mach number.

Trim Characteristics

The variations of the model trim characteristics with Mach number are shown in figure 8 as trim angle of attack, trim angle of sideslip, and trim lateral-force coefficient. These characteristics were determined when pitch coupling was negligible. The trim angle of attack remains relatively constant at subsonic and supersonic speeds at a value of 0.80°. The trim angle of sideslip is negative at subsonic speeds and becomes positive at supersonic speeds, while the trim lateral-force coefficient remains negative at both subsonic and supersonic speeds.

Lateral-Force Derivative

Two typical cross plots showing the variation of lateral-force coefficient with angle of sideslip are presented in figure 9. These cross plots are shown for $M = 0.86$ and $M = 1.42$ and indicate little difference in the slope of the lateral-force coefficient against angle of sideslip, C_{Y_β}. Presented in figure 10 is the variation of C_{Y_β} with Mach number which was determined from the cross plots of C_Y against β. The variation of C_{Y_β} with Mach number is presented only in the Mach number range when pitch coupling was negligible. Also shown in figure 10 is the vertical- and horizontal-tail contribution to C_{Y_β} calculated from the theory presented in reference 7. These results, along with an

estimate of C_{Y_β} of the wing-fuselage of about -0.1 per radian, indicate that at supersonic speeds the main contribution to C_{Y_β} is the vertical tail. The level of the measured C_{Y_β} is in good agreement with the calculations when due consideration, on a qualitative basis only, is given to possible effects such as aeroelasticity.

Vector Plots

As was previously mentioned, the gyro-type instrument used to measure rolling velocity became inoperative early in the flight of the model. During the major portion of the flight the model experienced a violent combined lateral-longitudinal motion; therefore, it was only possible to apply the vector method of analysis to the lateral motions at one Mach number, M = 1.50. These vector plots of the lateral equations of motion are presented in figure 11 and were obtained by the method presented in reference 1. The analysis was performed for an undamped natural circular frequency, ω, of 38.16 radians/sec; a total damping factor, a, of 1.81 per sec; an amplitude ratio of rolling velocity to angle of sideslip, $\frac{|\dot{\phi}|}{|\beta|}$, of 157.22 $\frac{\text{radians/sec}}{\text{degree}}$; and the phase of the rolling velocity to angle of sideslip, $\Phi_{\dot{\phi}\beta}$, of 131.56°.

Shown in figure 11(a) is the vector diagram of the lateral force equation. The solution of this equation yielded values of $\frac{|\dot{\psi}|}{|\beta|}$ and $\Phi_{\dot{\psi}\beta}$ which were used in the vector diagrams of the rolling and yawing moment equations. Figure 11(b) is the vector diagram of the rolling moment equation. In order to solve this equation, it was necessary to assume values for either C_{l_r} or C_{l_p}. Values of C_{l_r} were assumed and values of C_{l_β} and C_{l_p} were determined as functions of C_{l_r}: C_{l_r} = 0.10, 0.15, and 0.20. Shown on figure 11(b) are the vector lengths $C_{l_\beta}\frac{|\beta|}{|\beta|}$, $C_{l_p}\left(\frac{b}{2V}\right)\frac{|\dot{\phi}|}{|\beta|}$, and $C_{l_r}\left(\frac{b}{2V}\right)\frac{|\dot{\psi}|}{|\beta|}$. Listed below are the the values of C_{l_β} and C_{l_p} obtained from these vectors.

For values of

$C_{l_r} = 0.10$	$C_{l_\beta} = -0.078$	$C_{l_p} = -0.251$
$C_{l_r} = 0.15$	$C_{l_\beta} = -0.076$	$C_{l_p} = -0.236$
$C_{l_r} = 0.20$	$C_{l_\beta} = -0.074$	$C_{l_p} = -0.221$

The vector diagram for the yawing moment equation is presented in figure 11(c) and values of C_{n_β} and $\left(C_{n_r} - C_{n_{\dot\beta}}\right)$ were determined as functions of C_{n_p}; $C_{n_p} = -0.05$, 0, and 0.05. Shown on figure 11(c) are the vector lengths $C_{n_\beta}\frac{|\beta|}{|\beta|}$, $\left(C_{n_r} - C_{n_{\dot\beta}}\right)\left(\frac{b}{2V}\right)\frac{|\dot\psi|}{|\beta|}$, and $C_{n_p}\left(\frac{b}{2V}\right)\frac{|\dot\phi|}{|\beta|}$. Listed below are the values of C_{n_β} and $\left(C_{n_r} - C_{n_{\dot\beta}}\right)$ obtained from these vectors.

For values of

$C_{n_p} = -0.05$	$C_{n_\beta} = 0.171$	$\left(C_{n_r} - C_{n_{\dot\beta}}\right) = -0.310$
$C_{n_p} = 0$	$C_{n_\beta} = 0.178$	$\left(C_{n_r} - C_{n_{\dot\beta}}\right) = -0.151$
$C_{n_p} = 0.05$	$C_{n_\beta} = 0.185$	$\left(C_{n_r} - C_{n_{\dot\beta}}\right) = 0.013$

A comparison of C_{n_β} as determined from the vector method and the single-degree-of-freedom method is presented in figure 12. The single-degree-of-freedom value for C_{n_β} is determined directly from the periods of the Dutch roll oscillations, $C_{n_\beta} = \frac{4\pi^2 I_Z}{q_o S b P^2}$. The agreement between C_{n_β}, as determined from the single-degree-of-freedom method and the vector method, when $C_{n_p} = 0$ is good. The single-degree-of-freedom method for the determination of C_{n_β} shows that C_{n_β} is nearly constant at supersonic speeds. Also shown in figure 12 is the vertical- and horizontal-tail contribution to C_{n_β} calculated from the theory presented in figure 8. Available data on wing-body combinations similar to that of the model reported herein (except for the large wing-root fairings) indicate values of C_{n_β} of about -0.1 per radian. Agreement between C_{n_β} for the complete configuration based on these data and the measured data is good, considering possible effects such as loss in effectiveness of the vertical tail due to aeroelasticity. These results

are in agreement with the results discussed previously with regard to the lateral force derivative, C_{Y_β}.

Simulation of Combined Lateral-Longitudinal Motion

Simulation.- A simulation of the combined lateral-longitudinal motion experienced by the model at $M = 1.3$ and $q_o = 2{,}060$ lb/sq ft was attempted in order to determine the stability characteristics of the model while undergoing this maneuver. The model was assumed to have five degrees of freedom and the forces and moments acting on the model are described by the following equations of motion:

Rolling:

$$\dot{p} = \left(\frac{I_Y - I_Z}{I_X}\right)qr + \left(\frac{I_{XZ}}{I_X}\right)\dot{r} + \left(\frac{I_{XZ}}{I_X}\right)pq + \frac{q_o S b^2}{2VI_X} C_{l_p} p +$$

$$\frac{q_o S b^2}{2VI_X} C_{l_r} r + \frac{q_o S b}{I_X} C_{l_\beta}(\alpha)\beta + \frac{q_o S b}{I_X} C_{l_{PR}}$$

Pitching:

$$\dot{q} = \left(\frac{I_Z - I_X}{I_Y}\right)pr + \left(\frac{I_{XZ}}{I_Y}\right)r^2 - \left(\frac{I_{XZ}}{I_Y}\right)p^2 + \frac{q_o S \bar{c}^2}{2VI_Y} C_{m_q} q +$$

$$\frac{q_o S \bar{c}^2}{2VI_Y} C_{m_{\dot{\alpha}}} \dot{\alpha} + \frac{q_o S \bar{c}}{I_Y} C_{m_\alpha} \Delta\alpha + \frac{q_o S \bar{c}}{I_Y} C_{m_\beta} \beta$$

Yawing:

$$\dot{r} = \left(\frac{I_X - I_Y}{I_Z}\right)pq + \left(\frac{I_{XZ}}{I_Z}\right)\dot{p} - \left(\frac{I_{XZ}}{I_Z}\right)qr + \frac{q_o S b^2}{2VI_Z} C_{n_p} p +$$

$$\frac{q_o S b^2}{2VI_Z}\left(C_{n_r} - C_{n_{\dot{\beta}}}\right) r + \frac{q_o S b}{I_Z} C_{n_\beta}(\alpha)\beta + \frac{q_o S b}{I_Z} C_{n_{PR}}$$

Y-force:

$$\dot{\beta} = -r + \alpha p + \frac{q_o S}{mV} C_{Y_\beta} \beta + \frac{q_o S}{mV} C_{Y_{PR}}$$

Z-force:

$$\dot{\alpha} = q - p\beta - \frac{q_o S}{mV}\left(C_{L_\alpha} + C_D\right)\alpha$$

The terms $C_{l_\beta}(\alpha)$ and $C_{n_\beta}(\alpha)$ denote that C_{l_β} and C_{n_β} are variant with angle of attack. The terms $C_{l_{PR}}$, $C_{n_{PR}}$, and $C_{Y_{PR}}$ are, respectively, the rolling-moment coefficient, yawing-moment coefficient, and the lateral-force coefficient produced by the firing of the small pulse rocket motors.

Certain simplifying assumptions were made in the above equations. The gravity terms were neglected in the Y- and Z-force equations since the flight conditions of the model resulted in values of these terms which were very small. Aerodynamic terms in the Y-force and rolling moment equations due to rate of change of angle of sideslip were assumed to be zero, and in the yawing moment equation it was assumed $\dot{\psi} = \dot{\beta}$ so that C_{n_r} and $C_{n_{\dot{\beta}}}$ may be combined into one term. Further, it was assumed that in the Y-force equation the only aerodynamic term retained was that due to angle of sideslip since this quantity as measured contained the Y-force contributions due to $\dot{\psi}$ and $\dot{\phi}$ as well as β.

Since these equations of motion are nonlinear, an analog computer was employed in order to determine a solution. The aerodynamic characteristics of the model were estimated from various rocket model tests, wind-tunnel tests, and theory, whereas the mass characteristics used were those measured in the preflight tests of the model. The procedure employed in the simulation was to adjust systematically the estimated aerodynamic characteristics of the model until the solution of the equations of motion matched the flight test record of the combined motion. A considerable number of runs were made on the analog computer and changes in values of C_{m_q}, C_{n_p} (from estimated negative value of C_{n_p} to positive value of C_{n_p}), C_{l_p}, or C_{m_α} had large effects on the simulation, while wide variations in C_{Y_β}, $C_{l_{\dot{\beta}}}$, C_{l_r}, and $C_{m_{\dot{\alpha}}}$ had little effect. The best simulation obtained appears in figure 13. Zero time in this figure corresponds to the flight time when the second pulse

rocket was fired (t = 5.12 sec, see fig. 6). In order to achieve this simulation of the flight test record, a linear variation of C_{l_β} and C_{n_β} with angle of attack had to be incorporated into the equations of motion, but all other derivatives were considered invariant with angle of attack. The stability derivatives used are shown in table III.

The simulation shown in figure 13 is qualitatively good. Quantitative differences between the flight test results and the analog results indicate the need for more detailed studies of this type before any conclusions can be reached as to the accuracy of the derivatives obtained by this method.

Steady rolling analysis.- An analysis was made (based on ref. 6) of the combined lateral-longitudinal motion in order to determine how effective the method is in predicting the roll rate required for divergence. Values of the stability derivatives determined from the simulation were used in this analysis and the critical damping ratio in pitch was determined from a two-degree-of-freedom analysis and the critical damping ratio in yaw was also determined from a two-degree-of-freedom analysis. The results appear in figure 14 and indicate that the model would experience a divergence in angles of attack and sideslip when the rolling rate is between 39 and 42 radians/second. It was impossible to determine exactly the roll rate the model experienced when divergence occurred (see fig. 6), but the model did diverge at a roll rate considerably less than the maximum value recorded (-45 radians/sec).

It appears then that the analysis of reference 6 does predict that a divergence would occur, but due to the inaccuracy of the measured roll rate it is impossible to tell just how accurate the analysis is in predicting the exact value of the roll rate required for divergence. Also, as previously mentioned, the analysis accurately predicts the basic frequency of the model under steady rolling conditions.

Downwash and Sidewash

Data that have been obtained from an attempt to measure downwash and sidewash are presented herein to show what type of data can be expected from the measuring system used on this model. The method used to measure downwash and sidewash employed the nose air-flow indicator and an additional air-flow indicator that was sting mounted to the vertical tail. (See figs. 2 and 3.) The tail air-flow indicator measured the flow direction at a point which was in the plane of symmetry, above and ahead of the horizontal-tail surface.

The angular difference in the angle of attack and angle of sideslip between the free stream or nose air-flow indicator and the tail-mounted

air-flow indicator represents the angle of downwash and the angle of sidewash induced by the flow of air over the wings and fuselage.

The downwash data which were obtained from this test are shown in figure 15 and compared with various values obtained from previous experiments, theories, and calculations of references 8 to 12. The error in $d\epsilon/d\alpha$ was calculated by the method in reference 13 and was found to be from 12 to 14 percent of the measured value. The measured values of $d\epsilon/d\alpha$ from this test were taken from the largest amplitude of the angle of attack for each readable oscillation. The largest amplitude permitted the least amount of error in $d\epsilon/d\alpha$. The values obtained from this test are somewhat high in comparison to the reference values. It should be pointed out that the values obtained from this test were values for one specific point in the downwash field and not the average value over the horizontal tail; therefore, this higher value of $d\epsilon/d\alpha$ could possibly be justified.

The sidewash, $d\sigma/d\beta$, was determined by using the same procedure as for downwash. One test point was determined and its value was 0.19 at a Mach number of 1.412. The error involved was on the order of 26 percent of the measured value. This sidewash value is believed to be influenced entirely by sideslip and not by roll, as the roll parameter, $pb/2V$, was less than 0.003 at this Mach number. No comparison values for this type of sidewash were found; therefore, these data are included herein purely for academic reasons.

The dynamic pressure at a point above the tapered afterbody section of the fuselage between the horizontal and vertical tails was determined from a comparison of the measured values of the free-stream total head pressure and the total head pressure measured at this point by considering the static pressure to be constant and equal to the free-stream value. The data indicate that within the limits of accuracy of the measured quantities the dynamic pressure at a point above and to one side of the tapered afterbody section of the fuselage between the horizontal and vertical tails was equal to the free-stream dynamic pressure. ($\alpha < 1^\circ$; $\beta < 1^\circ$.)

CONCLUDING REMARKS

From the results of a flight test to determine the lateral stability characteristics of a rocket-propelled model of an airplane configuration having thin, highly tapered, 45° sweptback surfaces, the following conclusions are indicated:

At a Mach number of 1.3 the model experienced a violent combined lateral-longitudinal motion and large angles of sideslip and attack

together with large rolling velocities were recorded. Approximate simulation of this combined motion on an analog computer using nonlinear equations of motion with five degrees of freedom was made and indicated possible values of stability derivatives of the model while undergoing this maneuver.

The results from the analysis of the Dutch roll oscillations indicated that from a Mach number of 1.3 to a Mach number of 1.56 the lateral-force coefficient decreased and the directional stability was relatively constant with Mach number. It was only possible to apply the time-vector method of analysis to the lateral motions at one Mach number: a Mach number of 1.50. The value obtained for the directional-stability derivative agreed with the value obtained by the single-degree-of-freedom method.

Langley Aeronautical Laboratory,
National Advisory Committee for Aeronautics,
Langley Field, Va., January 6, 1955.

REFERENCES

1. D'Aiutolo, Charles T., and Henning, Allen B.: Lateral Stability Characteristics at Low Lift Between Mach Numbers of 0.85 and 1.15 of a Rocket-Propelled Model of a Supersonic Airplane Configuration Having a Tapered Wing With Circular-Arc Sections and 40° Sweepback. NACA RM L55A31, 1955.

2. Mitchell, Jesse L., and Peck, Robert F.: Investigation of the Lateral Stability Characteristics of the Douglas X-3 Configuration at Mach Numbers From 0.6 to 1.1 by Means of a Rocket-Propelled Model. NACA RM L54L20, 1955.

3. Jones, B. Melvill: Dynamics of the Aeroplane. The Asymmetric or Lateral Moments. Vol. V of Aerodynamic Theory, div. N, ch. III, secs. 10 and 21, W. F. Durand, ed., Julius Springer (Berlin), 1935, pp. 61, 71-72.

4. Ikard, Wallace L.: An Air-Flow-Direction Pickup Suitable for Telemetering Use on Pilotless Aircraft. NACA RM L53K16, 1954.

5. Harris, Orville R.: Determination of the Rate of Roll of Pilotless Aircraft Research Models by Means of Polarized Radio Waves. NACA TN 2023, 1950.

6. Phillips, William H.: Effect of Steady Rolling on Longitudinal and Directional Stability. NACA TN 1627, 1948.

7. Malvestuto, Frank S., Jr.: Theoretical Supersonic Force and Moment Coefficients on a Sideslipping Vertical- and Horizontal-Tail Combination With Subsonic Leading Edges and Supersonic Trailing Edges. NACA TN 3071, 1954.

8. Osborne, Robert S.: High-Speed Wind-Tunnel Investigation of the Longitudinal Stability and Control Characteristics of a 1/16-Scale Model of the D-558-2 Research Airplane at High Subsonic Mach Numbers and at a Mach Number of 1.2. NACA RM L9C04, 1949.

9. Stephenson, Jack D., Selan, Ralph, and Bandettin, Angelo: A Comparison at Mach Numbers Up to 0.92 of the Calculated and Experimental Downwash and Wake Characteristics at Various Horizontal Tail Heights Behind a Wing with 45° of Sweepback. NACA RM A55D27a, 1955.

10. Parks, James H.: Transonic Longitudinal Aerodynamic Effects of Sweeping Up the Rear of the Fuselage of a Rocket-Propelled Airplane Model Having No Horizontal Tail. NACA RM L54K12, 1955.

11. Schlichting, H.: Aerodynamics of the Mutual Influence of Aircraft Parts (Interference). Library Translation No. 275, British R.A.E., Oct. 1948.

12. Diederich, Franklin W.: Charts and Tables for Use in Calculations of Downwash of Wings of Arbitrary Plan Form. NACA TN 2353, 1951.

13. Scarborough, James B.: Numerical Mathematical Analysis. Second ed., The Johns Hopkins Press (Baltimore), 1950, pp. 428-438.

TABLE I.- MASS AND GEOMETRIC CHARACTERISTICS

Wing:	
Total area, sq ft	4.41
Span, ft	4.20
Aspect ratio	4
Taper ratio	0.2
Sweep of quarter-chord line, deg	45
Mean aerodynamic chord, ft	1.208
Dihedral, deg	0
Incidence, deg	0
Airfoil section, parallel to free stream	65A004
Horizontal tail:	
Total area, sq ft	0.881
Span, ft	1.875
Aspect ratio	4
Taper ratio	0.2
Sweep of quarter-chord line, deg	45
Airfoil section, parallel to free stream	65A004
Vertical tail:	
Area, sq ft (total included area to center line of model)	0.885
Span, ft	1.187
Aspect ratio	1.59
Taper ratio	0.172
Sweep of quarter-chord line, deg	45
Airfoil section, parallel to free stream	65A004
Fuselage:	
Length, ft	6.33
Fineness ratio	10.72
General:	
Weight, lb	99.75
I_X, slug-ft^2	0.55
I_Y, slug-ft^2	6.23
I_Z, slug-ft^2	6.79
I_{XZ}, slug-ft^2	0.0655
Center-of-gravity location	$0.193\bar{c}$
Wing first bending frequency, cps	46.5
Wing second bending frequency, cps	160
Horizontal tail first bending frequency, cps	112

TABLE II.- ESTIMATED ACCURACY OF BASIC QUANTITIES

[Values shown are positive or negative quantities]

Mach number	Accuracy of -											
	W, percent	I_Z, percent	I_X, percent	I_{XZ}, percent	M, percent	q_o, percent	ω, percent	$\frac{\lvert\dot{\phi}\rvert}{\lvert\beta\rvert}$ percent	$\frac{\lvert A_T/g\rvert}{\lvert\beta\rvert}$, percent	$\Phi_{\dot{\phi}\beta}$, deg	α, deg	a, sec^{-1}
1.50	0.5	2.0	2.0	16.0	1.0	2.0	3.0	3.0	2.0	3.0	0.5	0.1

TABLE III.- VALUES OF DERIVATIVES AS OBTAINED FROM SIMULATION OF COUPLED MOTION. M = 1.3

[All values for zero angle of attack. All derivatives in radian measure.]

$C_{n_\beta} = 0.25$	$C_{n_r} - C_{n_{\dot{\beta}}} = -0.40$
$C_{l_\beta} = -0.08$	$C_{l_r} = 0.10$
$C_{Y_\beta} = -0.76$	$C_{L_\alpha} = 3.3$
$C_{n_p} = 0.20$	$C_{m_\alpha} = -0.86$
$C_{l_p} = -0.32$	$C_{m_q} = -4.7$
$C_{m_\beta} = 0.17$	$C_{m_{\dot{\alpha}}} = 3.0$
	$C_D = 0.035$

Note: C_{l_β} and C_{n_β} were assumed variant with angle of attack, that is, C_{l_β} increased with angle of attack until at $\alpha = 7^\circ$, $C_{l_\beta} = -0.16$; while C_{n_β} decreased with increasing angle of attack and at $\alpha = 5^\circ$, $C_{n_\beta} = 0$.

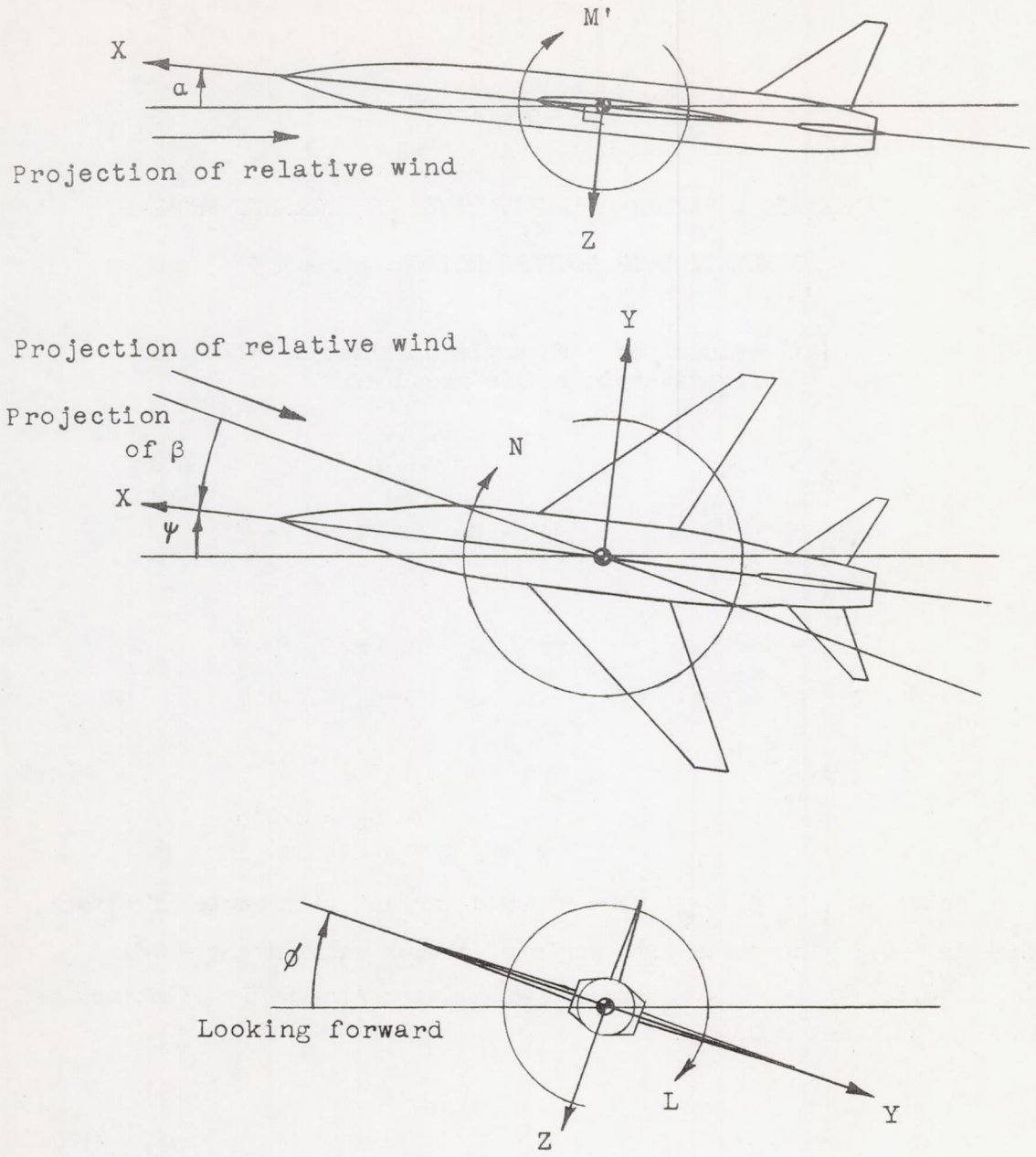

Figure 1.- Sketch showing the body-axes system. Each view presents a plane of the axes system as viewed along the third axis. Arrows indicate positive direction of forces, moments, and angles.

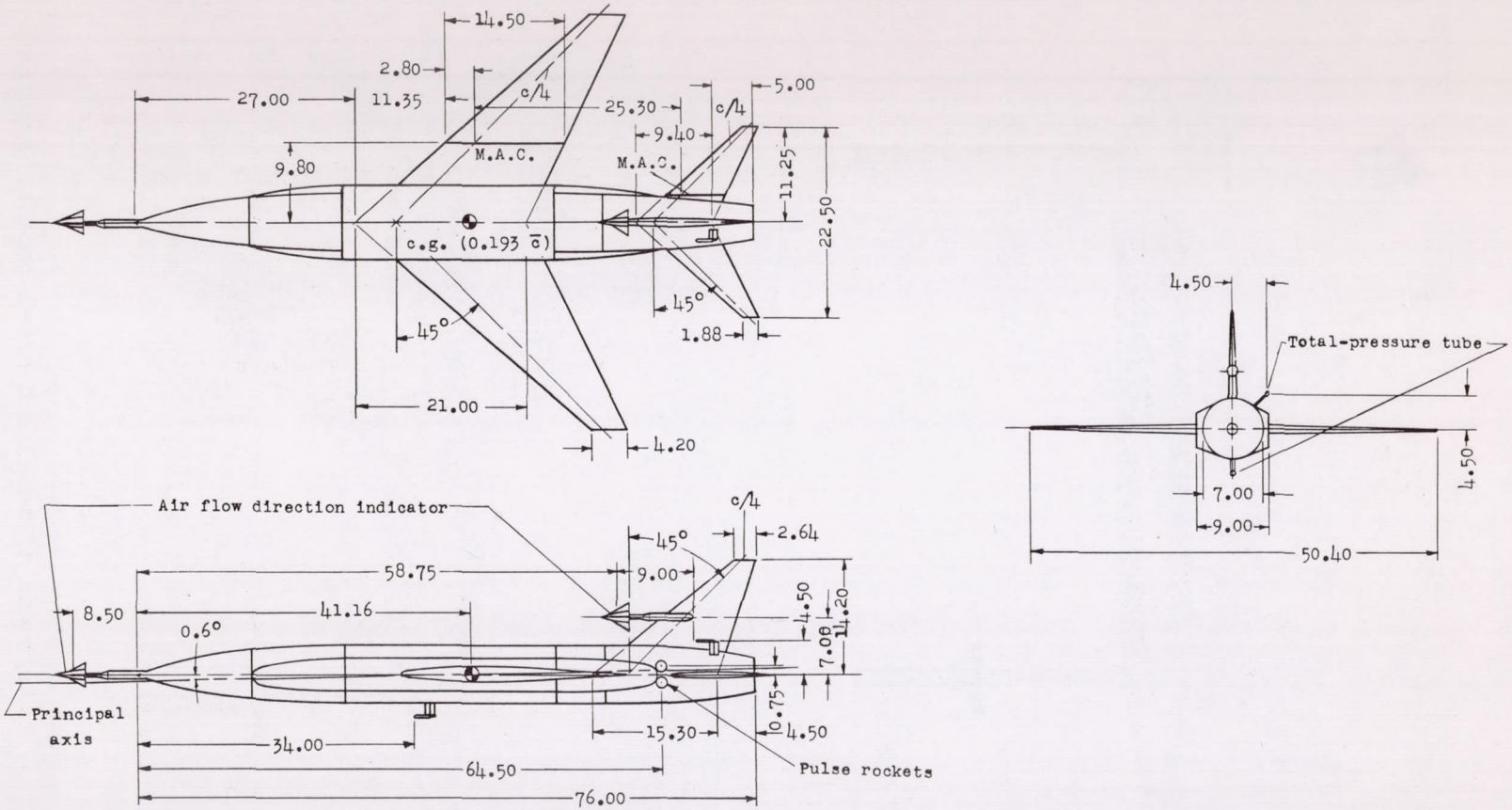

Figure 2.- General arrangement of model. All dimensions are in inches unless otherwise noted.

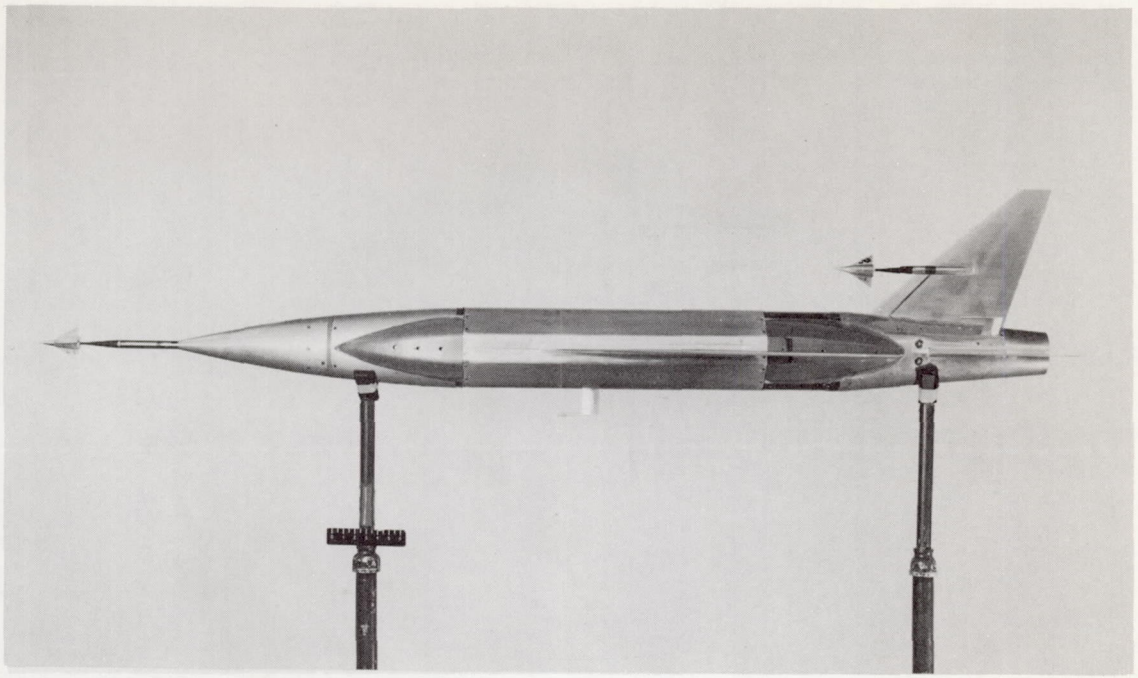

(a) Side view. L-82441.1

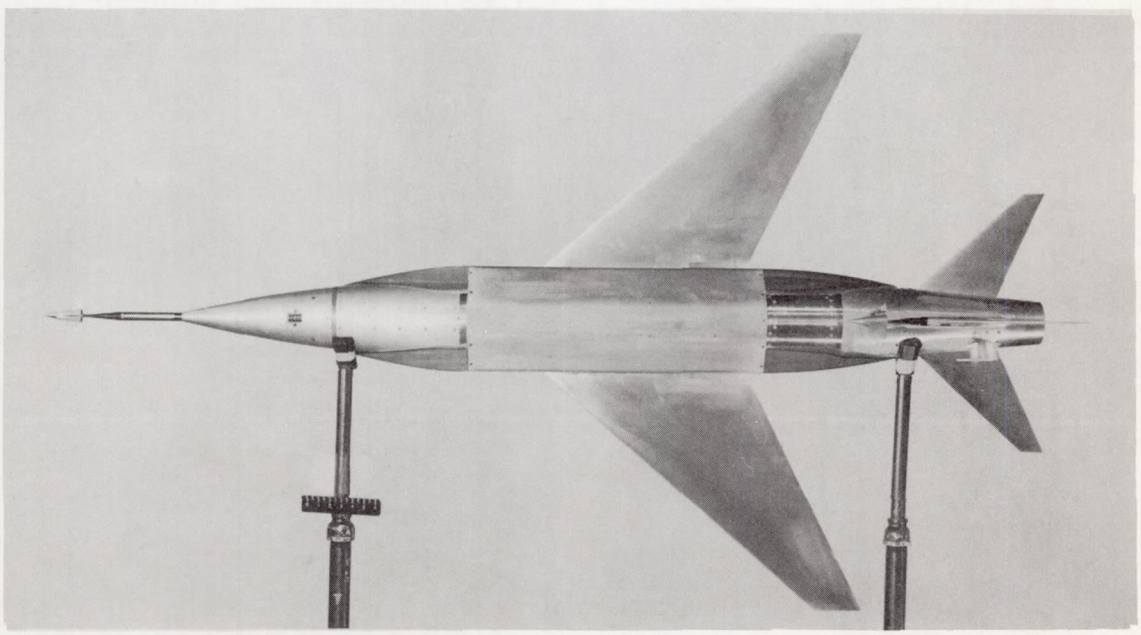

(b) Top view. L-82439.1

Figure 3.- Photographs of model and model-booster combination.

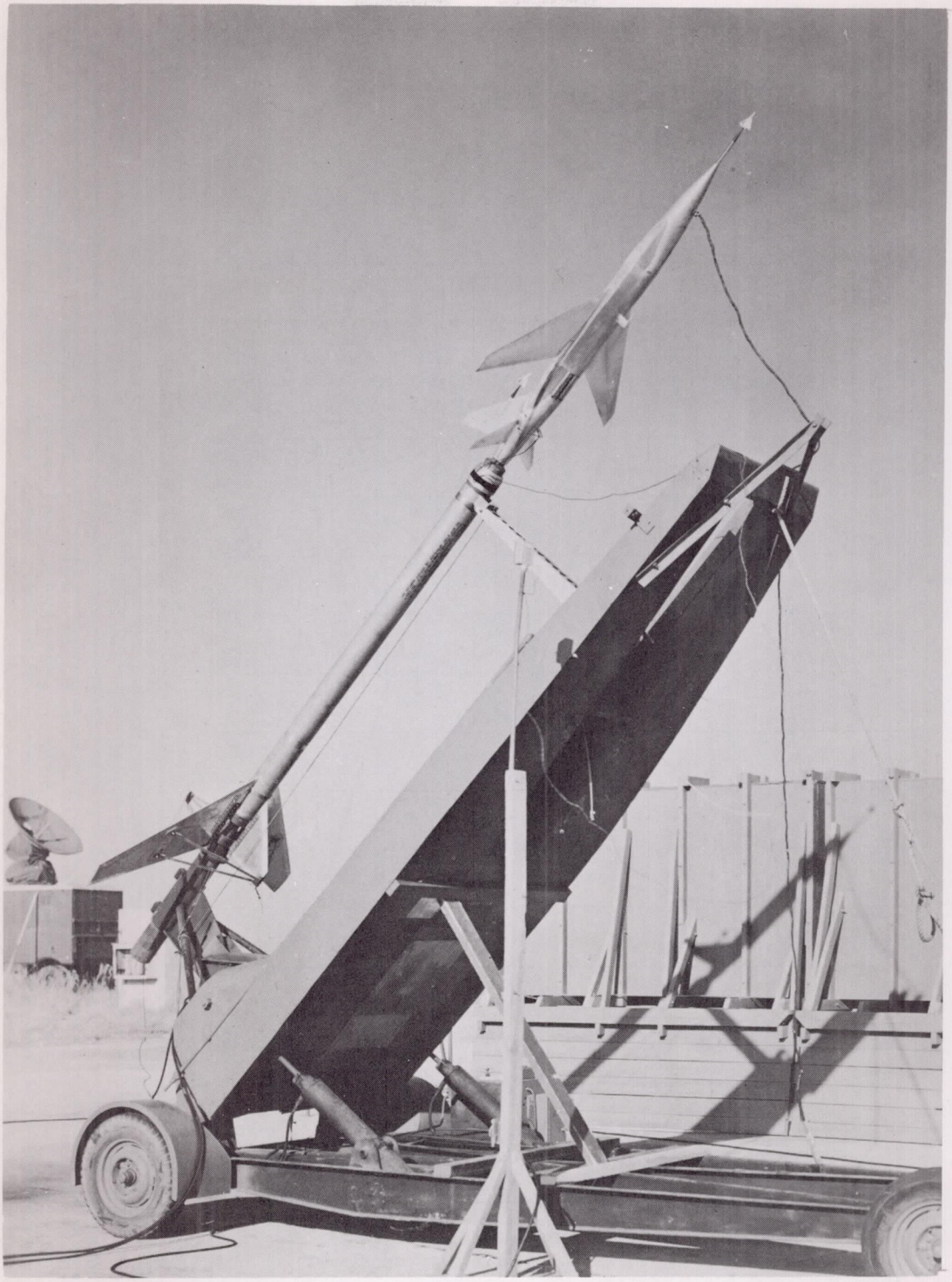

(c) Model-booster combination on launcher.

Figure 3.- Concluded. L-82832.1

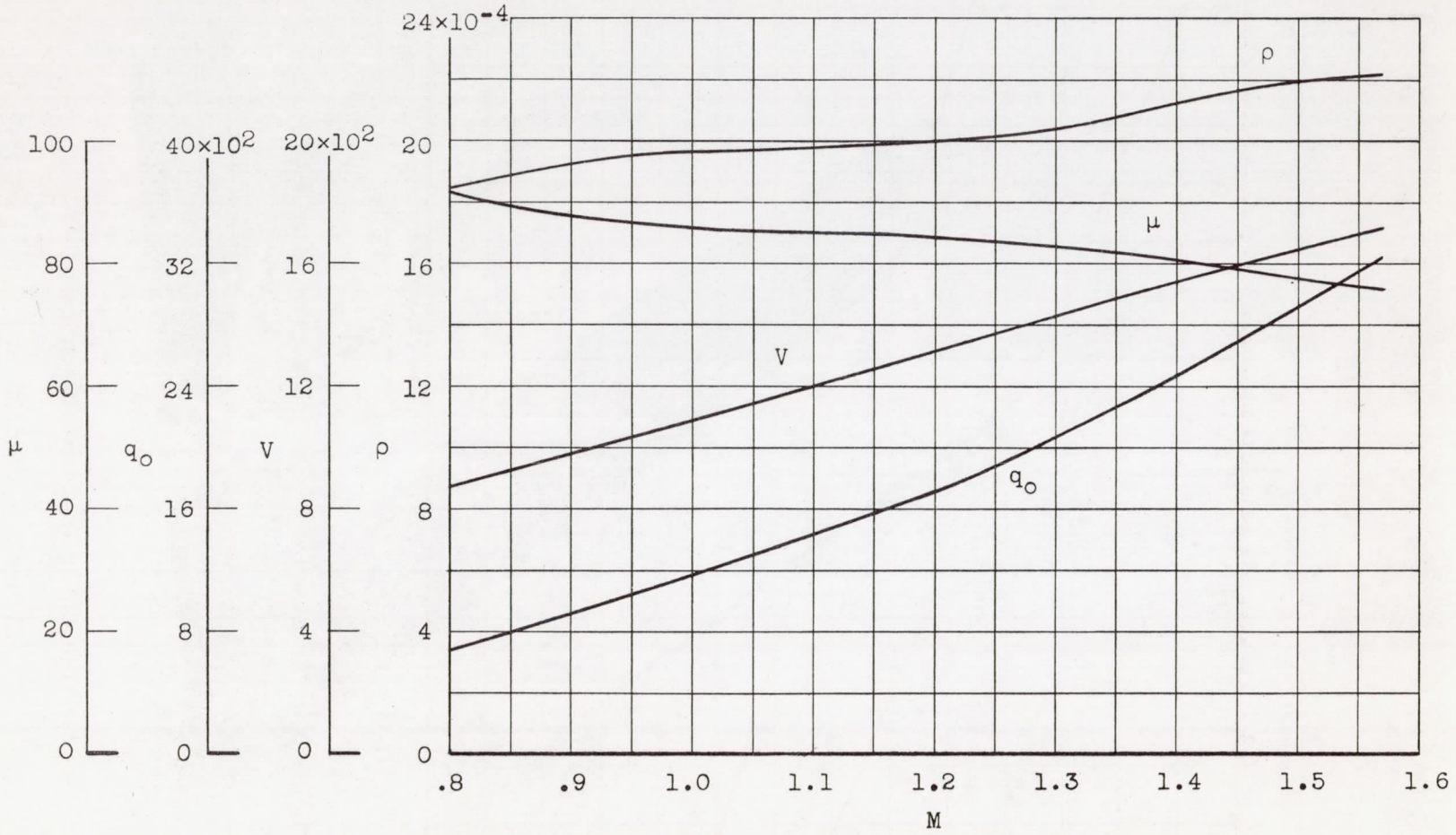

Figure 4.- Variation of relative density factor, dynamic pressure, velocity, and air density with Mach number.

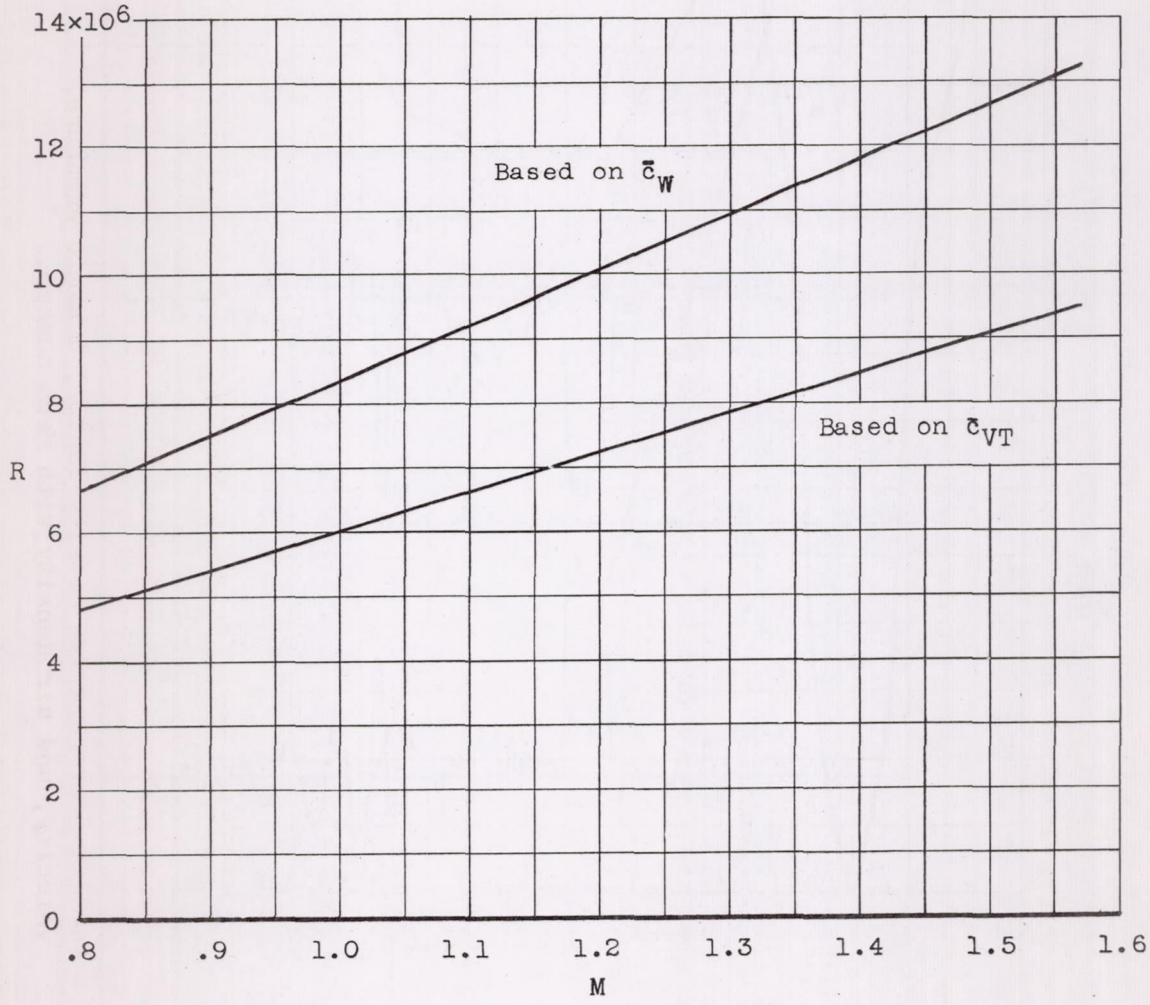

Figure 5.- Variation of Reynolds number with Mach number.

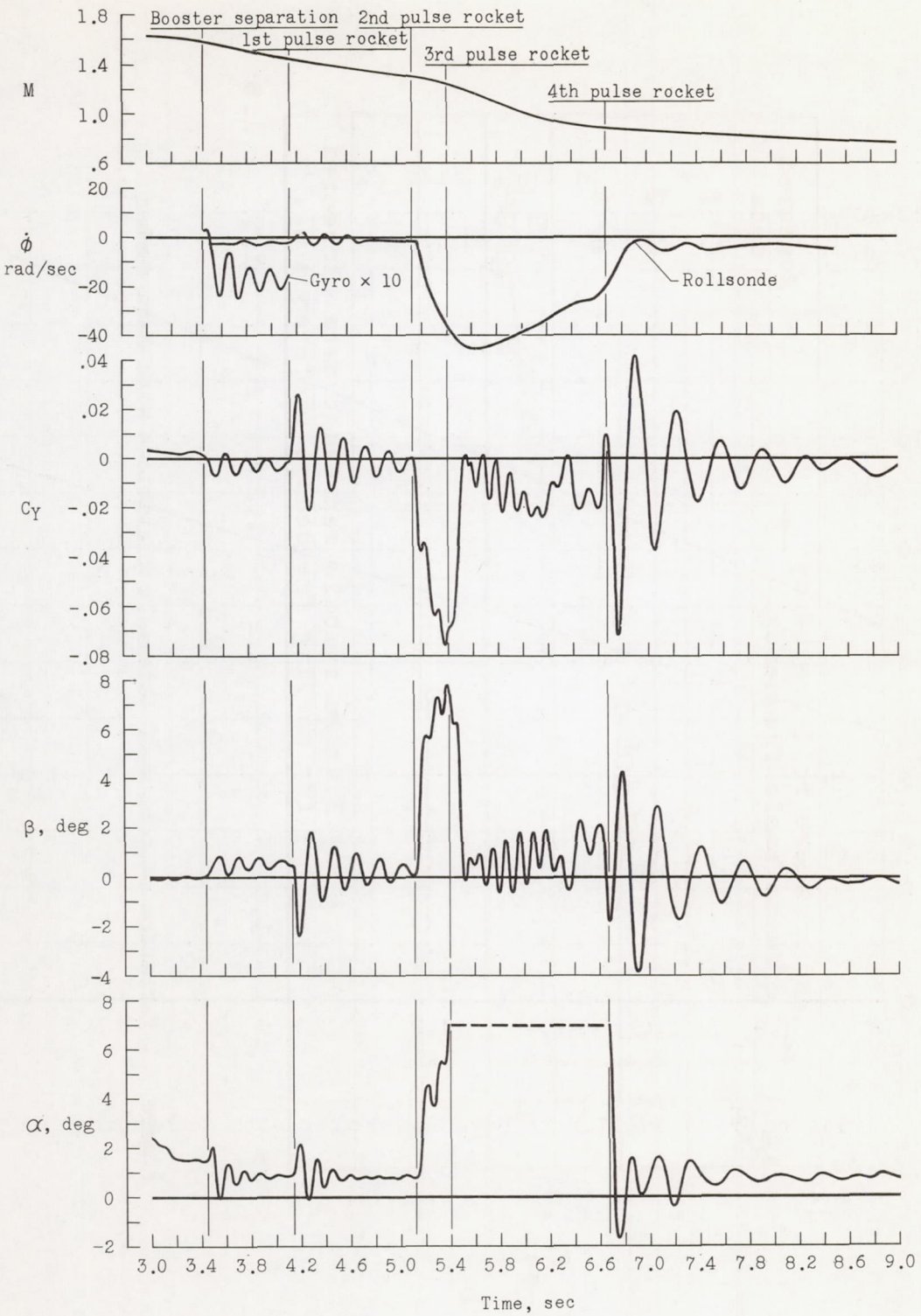

Figure 6.- Time history of model flight.

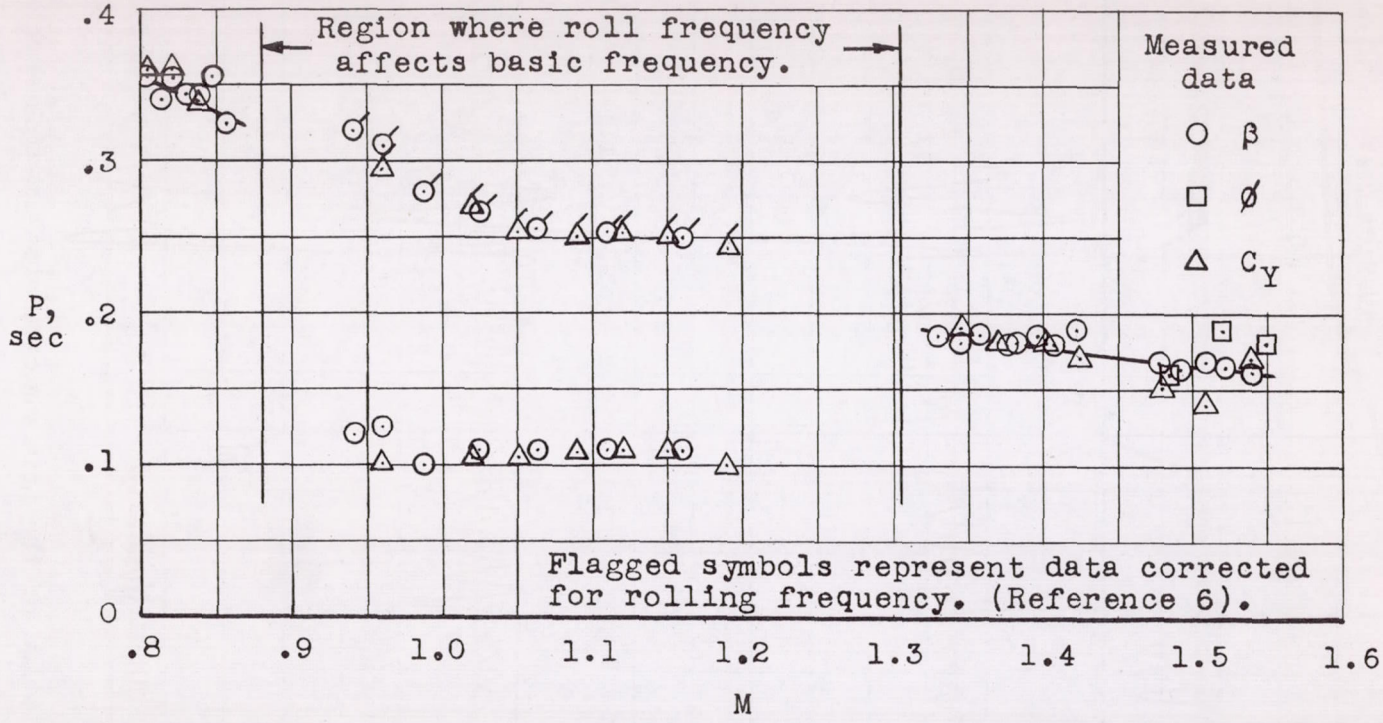

Figure 7.- Variation of period of lateral oscillations with Mach number.

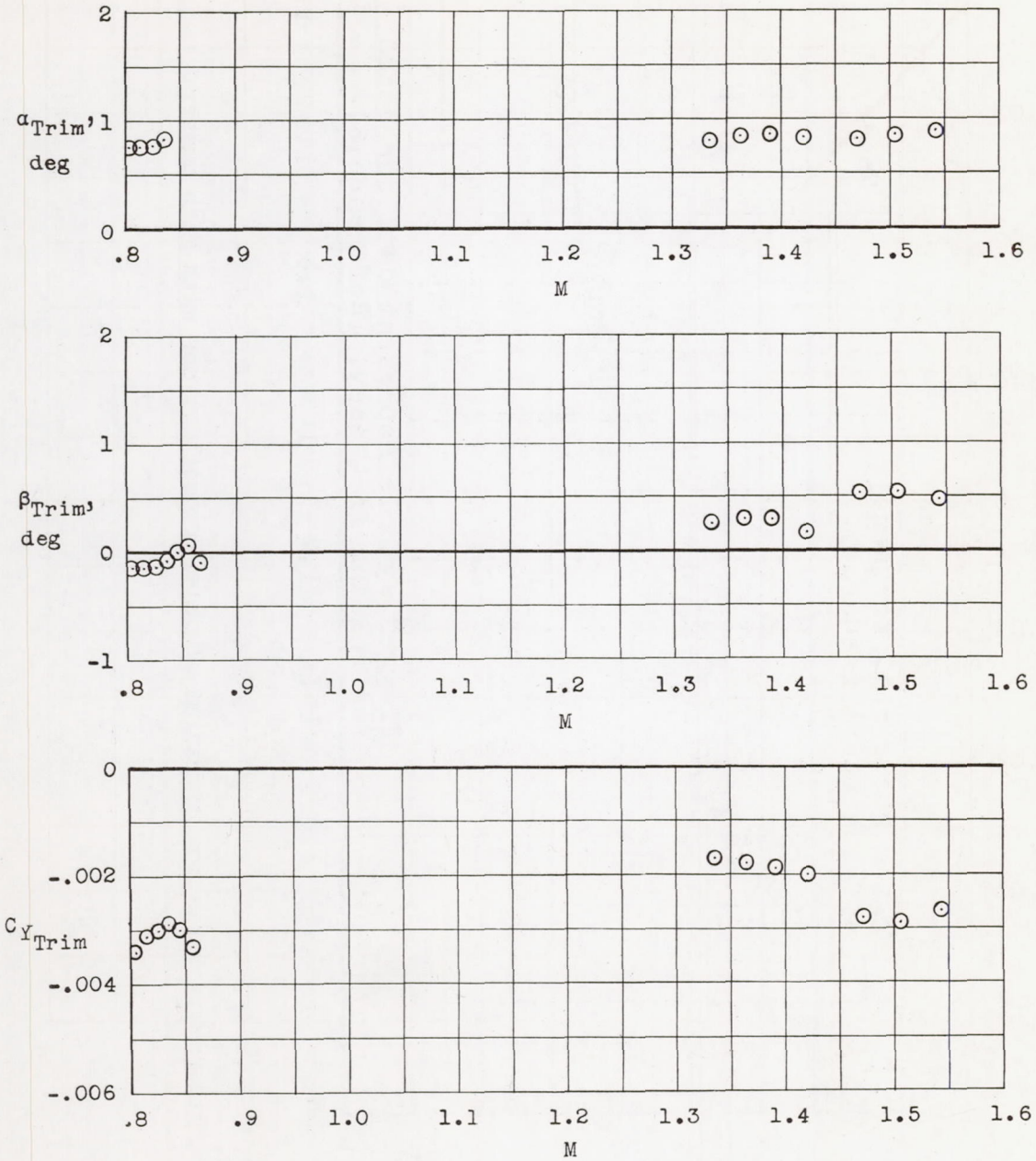

Figure 8.- Variation of the trim characteristics with Mach number.

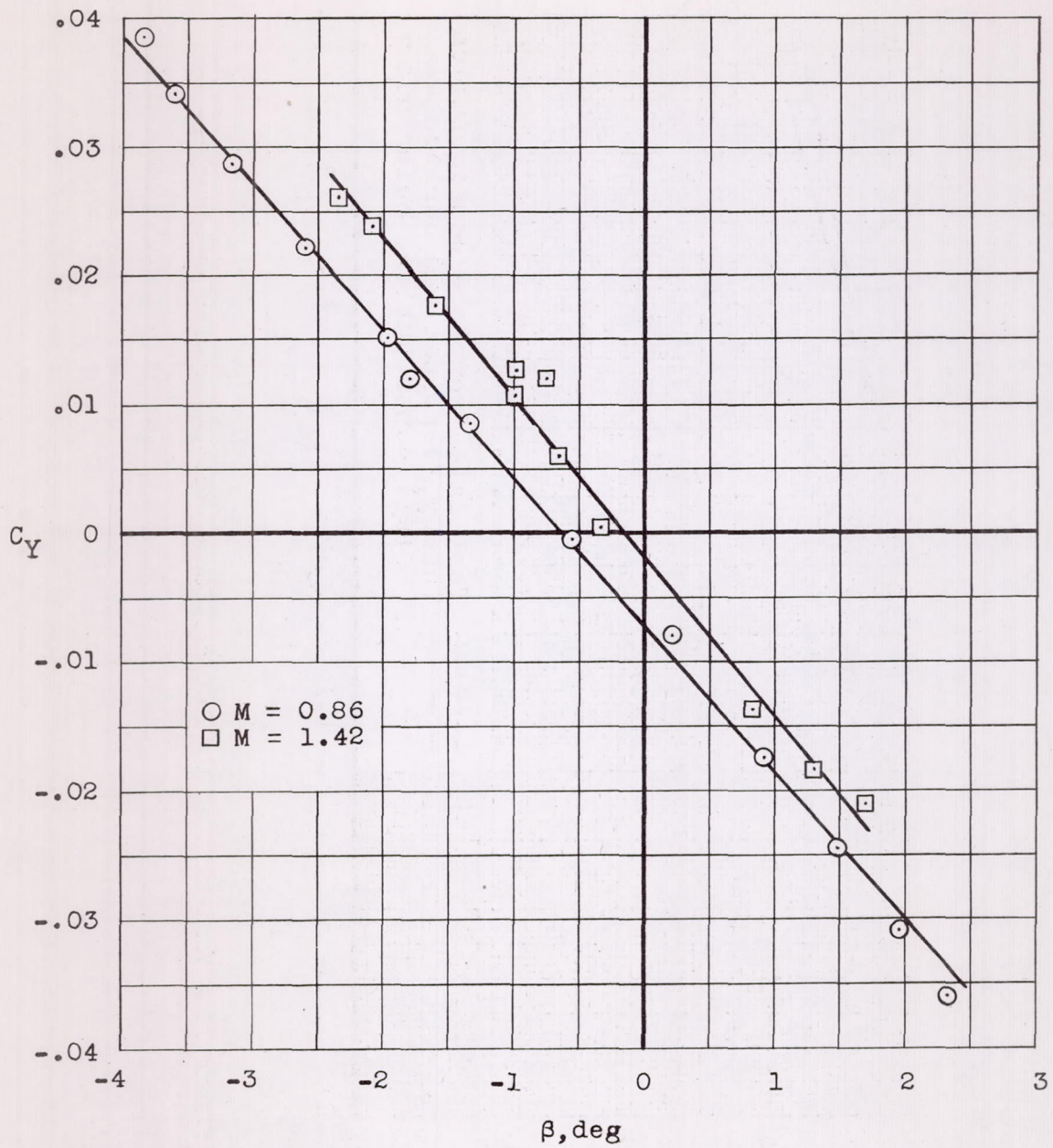

Figure 9.- Typical variation of side force coefficient with angle of sideslip.

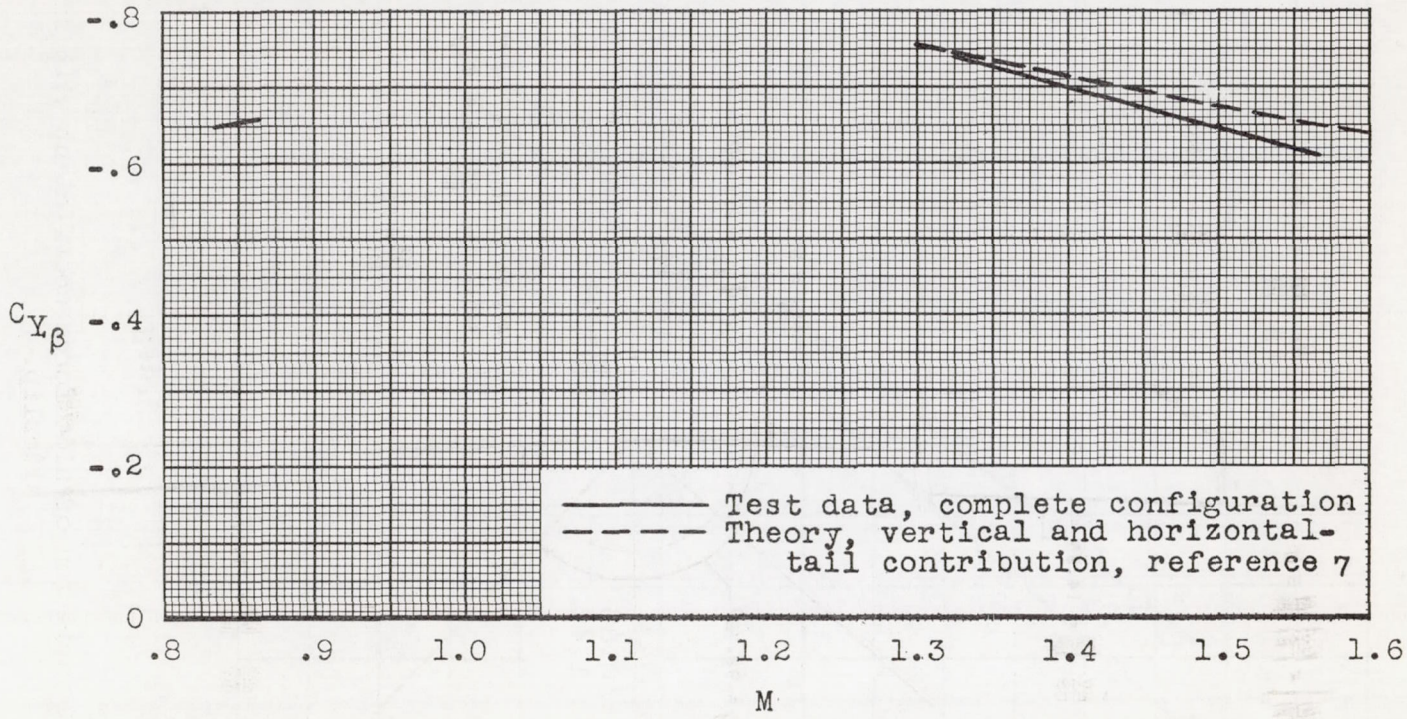

Figure 10.- Variation of the lateral-force derivative with Mach number.

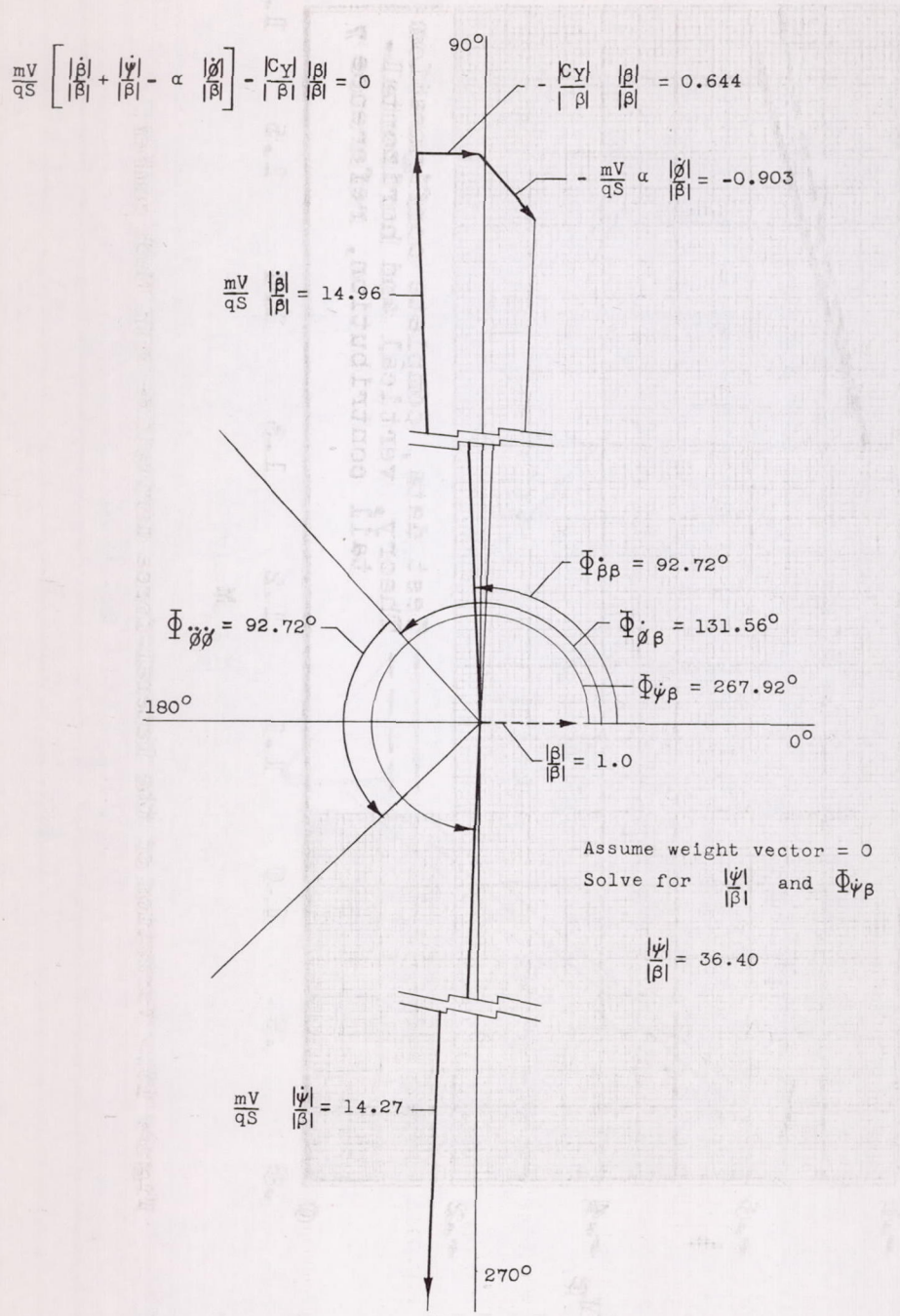

(a) Lateral-force equation.

Figure 11.- Vector plots for the calculation of the lateral stability derivatives at M = 1.5.

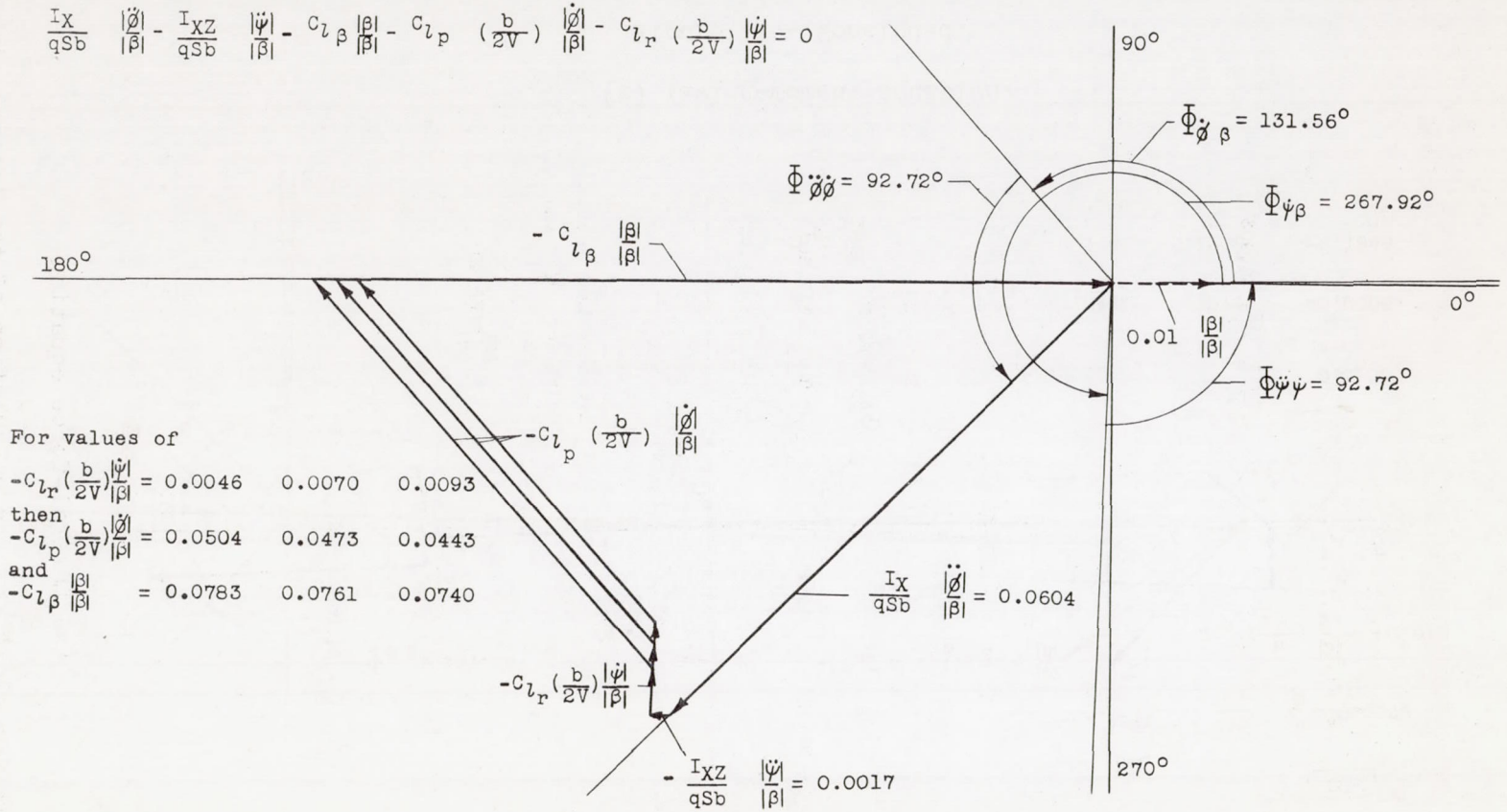

(b) Rolling-moment equation.

Figure 11.- Continued.

$$\frac{I_Z}{qSb}\frac{|\ddot{\psi}|}{|\beta|} - \frac{I_{XZ}}{qSb}\frac{|\ddot{\phi}|}{|\beta|} - C_{n_p}\left(\frac{b}{2V}\right)\frac{|\dot{\phi}|}{|\beta|} - \left(C_{n_r} - C_{n_{\dot{\beta}}}\right)\left(\frac{b}{2V}\right)\frac{|\dot{\psi}|}{|\beta|} - C_{n_\beta}\frac{|\beta|}{|\beta|} = 0$$

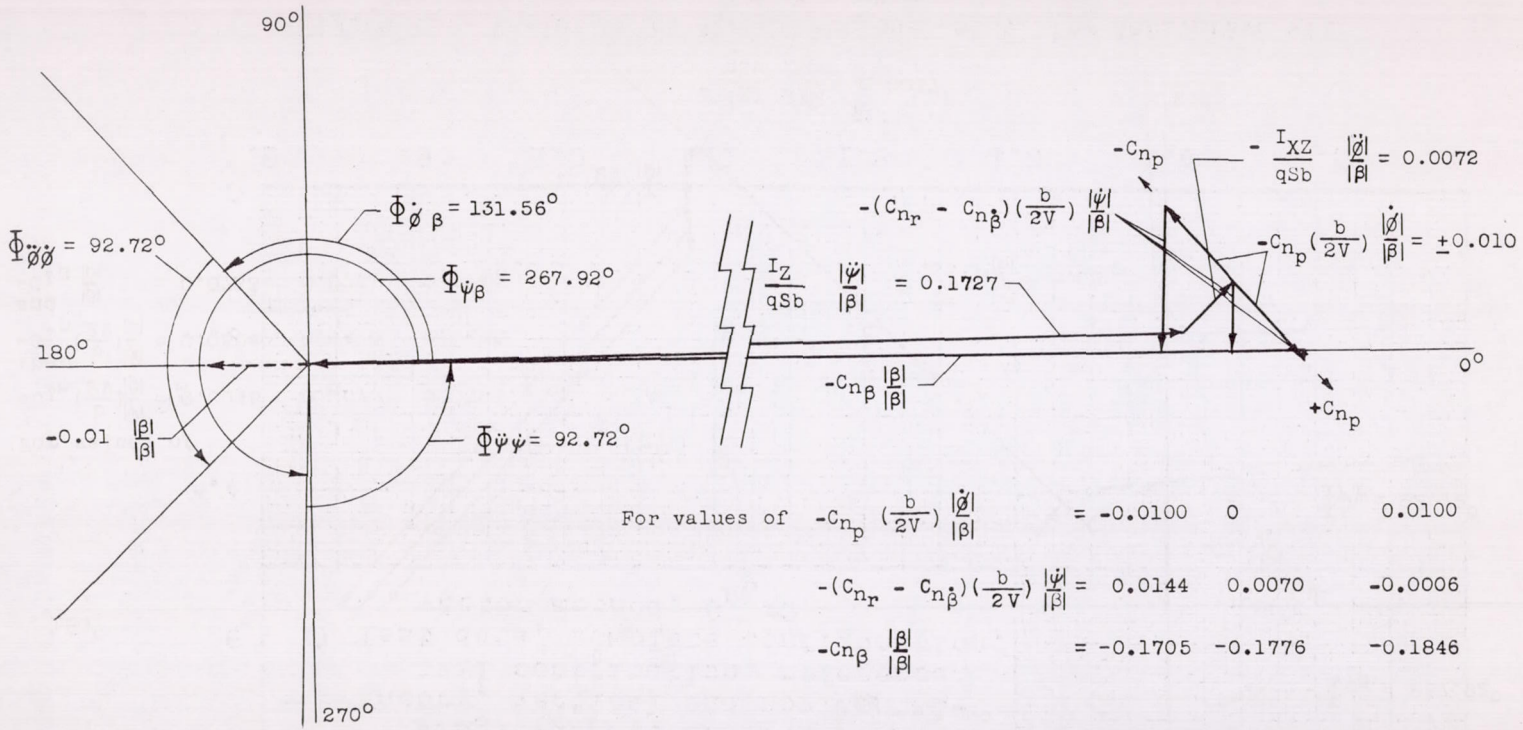

For values of

$-C_{n_p}\left(\frac{b}{2V}\right)\frac{\lvert\dot{\phi}\rvert}{\lvert\beta\rvert}$	= -0.0100	0	0.0100
$-\left(C_{n_r} - C_{n_{\dot{\beta}}}\right)\left(\frac{b}{2V}\right)\frac{\lvert\dot{\psi}\rvert}{\lvert\beta\rvert}$	= 0.0144	0.0070	-0.0006
$-C_{n_\beta}\frac{\lvert\beta\rvert}{\lvert\beta\rvert}$	= -0.1705	-0.1776	-0.1846

(c) Yawing-moment equation.

Figure 11.- Concluded.

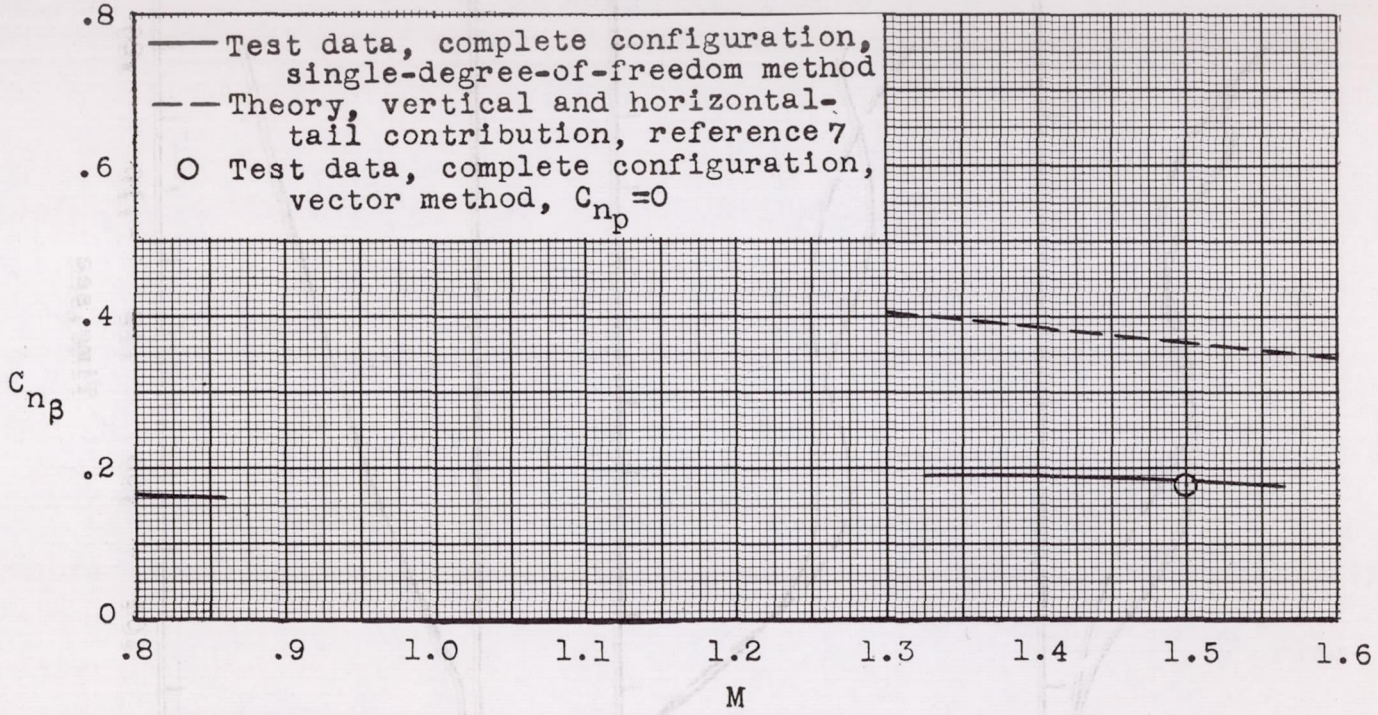

Figure 12.- Variation of the directional-stability derivative with Mach number.

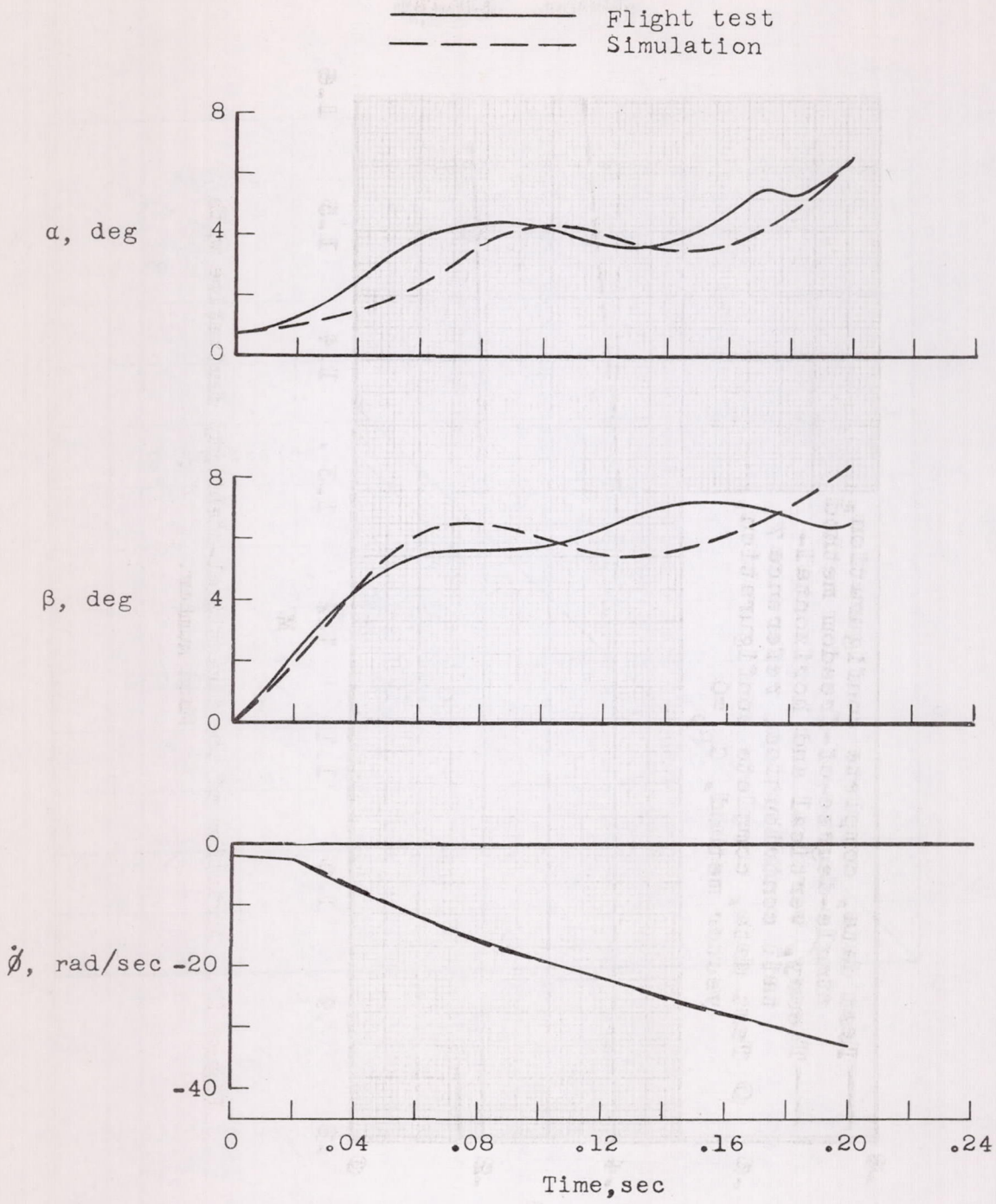

Figure 13.- Comparison of flight test and simulation results of combined lateral-longitudinal motion. M = 1.3; q_o = 2,060 lb/sq ft.

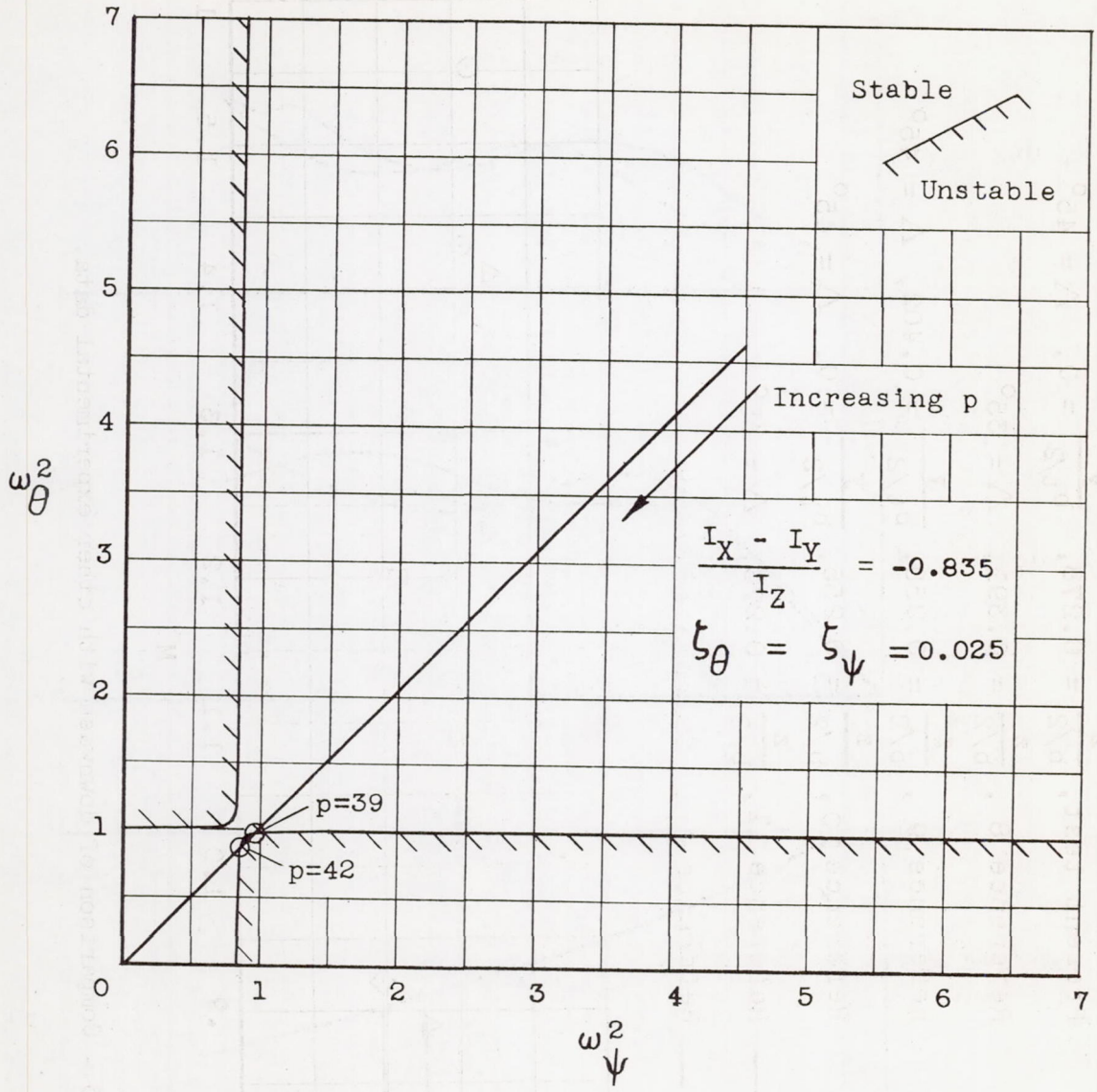

Figure 14.- Effect of steady rolling on the pitch and yaw stabilities. M = 1.3.

○ Present test, $\frac{z}{b/2} = 0.278$, $\frac{y}{b_{t/2}} = 0$, $\Lambda = 45^\circ$

□ Reference 8, $\frac{z}{b/2} = 0.391$, $\Lambda = 35^\circ$

◇ Reference 9, $\frac{z}{b/2} = 0.258$, $\frac{y}{b_{t/2}} = 0.402$, $\Lambda = 45^\circ$

△ Reference 10, $\frac{z}{b/2} = 0.255$, $\frac{y}{b_{t/2}} = 0$, $\Lambda = 45^\circ$

——— Reference 11, $\frac{z}{b/2} = 0.278$, $\Lambda = 45^\circ$

— — — Reference 12, Calculated value

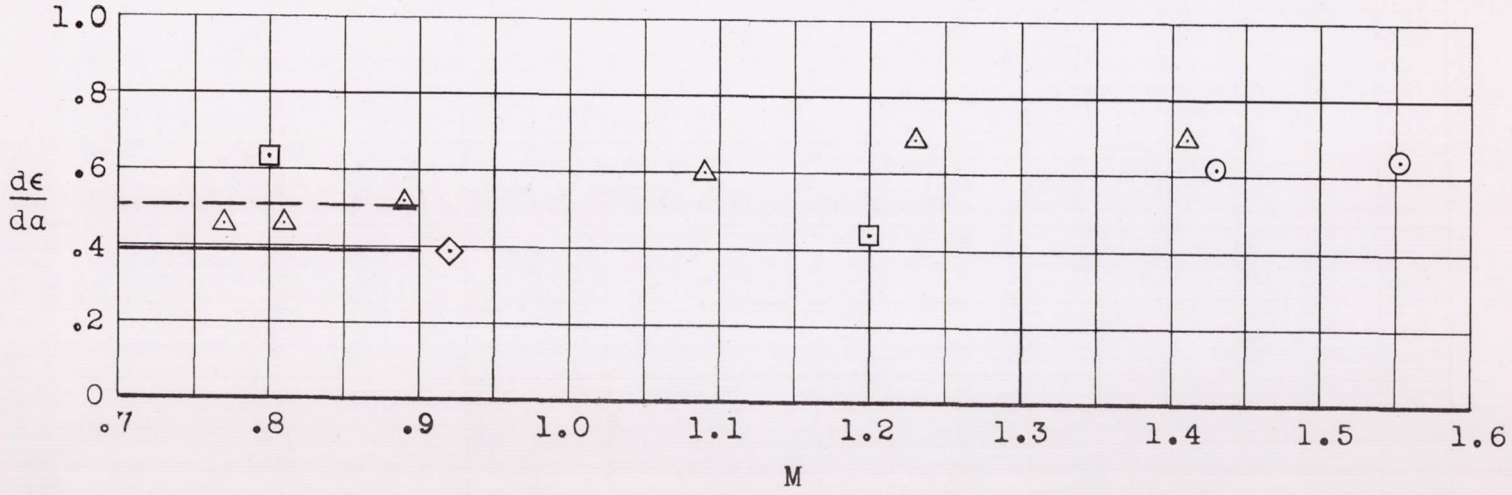

Figure 15.- Comparison of downwash with other experimental data.